Transient Artifact Reduction Algorithm (TARA) using Sparse Optimization

Tong Zhang,[1] Harry L. Graber,[2] Randall L. Barbour,[2] and Ivan W. Selesnick[1]

(1) Dept. Electrical and Computer Engineering, NYU School of Engineering, Brooklyn, NY 11201, USA

(2) Department of Pathology, SUNY Downstate Medical Center, Brooklyn, NY 11203, USA

Abstract

We address suppression of artifacts in NIRS time-series imaging. We report a fast algorithm, combining sparse optimization and filtering, that jointly estimates two explicitly modeled artifact types: transient disruptions and step discontinuities.

1. Introduction

This work addresses the attenuation of artifacts arising in biomedical time-series, such as those acquired using near infrared spectroscopic (NIRS) imaging devices [1]. We model the measured time series, $y(t)$, as

$$y(t) = f(t) + x_1(t) + x_2(t) + w(t) \quad t \in \mathbb{R}, \qquad (1)$$

- $f(t)$ is a low-pass signal, i.e., $\mathbf{H}f \approx 0$ for HPF $\mathbf{H}$.
- $x_1(t)$ is a 'Type 1' artifact signal, intended to model spikes. We model a Type 1 artifact signal as being sparse and having a sparse derivative. It adheres to a baseline value of zero.
- $x_2(t)$ is a 'Type 2' artifact signal, intended to model additive step discontinuities. We model a Type 2 artifact signal as having a sparse derivative. It is composed of (approximate) step discontinuities.
- $w(t)$ is white Gaussian noise.

Both Type 1 and Type 2 artifacts are observed in NIRS time series [3].

We devise the 'Transient Artifact Reduction Algorithm' (TARA) to estimate both artifacts types simultaneously, so they can be subtracted from the raw data. TARA has high computational efficiency and low memory requirements.

2. Problem Formulation

We address the problem in the discrete-time setting. We propose the optimization problem

$$\{\hat{\mathbf{x}}_1, \hat{\mathbf{x}}_2\} = \arg\min_{\mathbf{x}_1, \mathbf{x}_2} \Big\{ \frac{1}{2} \|\mathbf{H}(\mathbf{y} - \mathbf{x}_1 - \mathbf{x}_2)\|_2^2 + \lambda_0 \sum_n \phi_0([\mathbf{x}_1]_n) + \lambda_1 \sum_n \phi_1([\mathbf{D}\mathbf{x}_1]_n) + \lambda_2 \sum_n \phi_2([\mathbf{D}\mathbf{x}_2]_n) \Big\}, \quad \lambda_i > 0. \qquad (2)$$

$\mathbf{H}$ denotes the high-pass filter suppressing the low-pass signal $\mathbf{f}$. $\mathbf{D}$ is discrete-time first-order difference operator, given by $[\mathbf{D}\mathbf{x}]_n = [\mathbf{x}]_{n+1} - [\mathbf{x}]_n$. The low-pass signal is estimated as

$$\hat{\mathbf{f}} = \mathbf{L}(\mathbf{y} - \hat{\mathbf{x}}_1 - \hat{\mathbf{x}}_2) \qquad (3)$$

where $\mathbf{L}$ denotes the low-pass filter $\mathbf{L} = \mathbf{I} - \mathbf{H}$.

The functions ϕ_i are chosen to promote sparsity, e.g.,

$$\phi(u) = \frac{1}{a} \log(1 + a|u|), \quad a > 0.$$

The high-pass filter, $\mathbf{H}$, is implemented as

$$\mathbf{H} = \mathbf{B}\mathbf{A}^{-1}, \qquad (4)$$

where $\mathbf{A}$ and $\mathbf{B}$ are banded matrices.

3. Example 1

We illustrate a special case of TARA for Type 1 artifacts only ($\mathbf{x}_2$ is absent from (2)). We use a simulated signal (Fig. 1(a)) consisting of several additive step-transients. With $(\lambda_0, \lambda_1) = (\lambda_0^*, 0)$, $\hat{\mathbf{x}}$ deviates infrequently from the baseline value of zero (Fig. 2(a)). With $(\lambda_0, \lambda_1) = (0, \lambda_1^*)$, it is approximately piecewise constant but does not adhere to a baseline of zero (Fig. 2(b)). With

$$(\lambda_0, \lambda_1) = (\theta\lambda_0^*, (1-\theta)\lambda_1^*), \quad 0 \leqslant \theta \leqslant 1, \qquad (5)$$

with θ tuned to 0.3, it is reasonably sparse and has a sparse derivative (Fig. 2(c)). The interpolation given by (5) provides a trade-off.

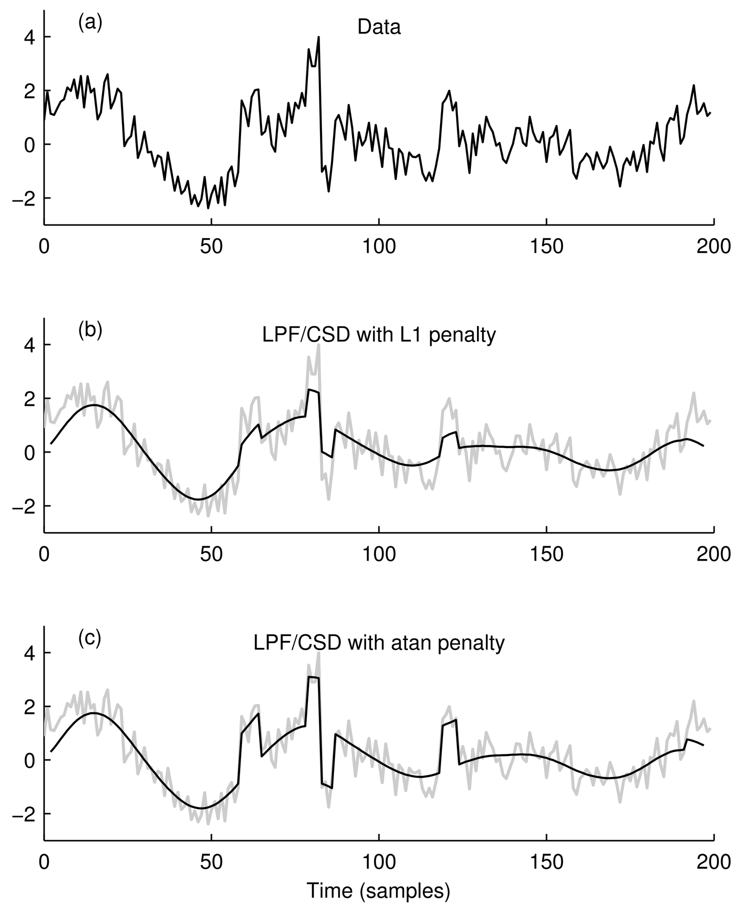

Figure 1: *(a) Simulated data. Processing with the ℓ_1-norm penalty (b) and the arctangent penalty (c).*

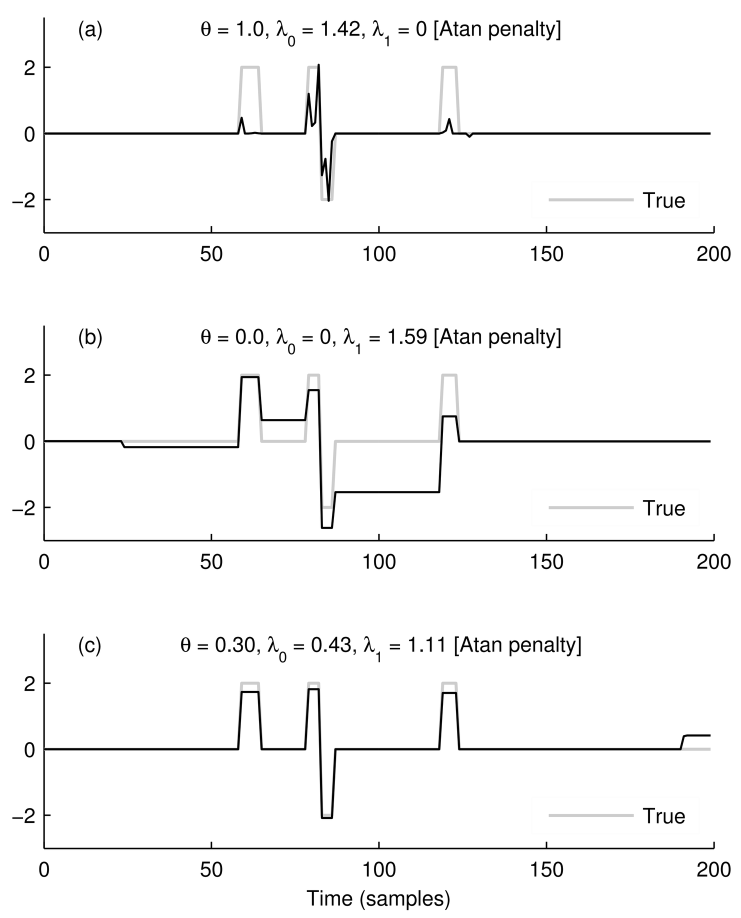

Figure 2: *Estimated transient signals, $\hat{\mathbf{x}}$, obtained with various (λ_0, λ_1). (a) $\theta = 1$. (b) $\theta = 0$. (c) $\theta = 0.3$.*

4. Example 2

This example shows TARA, for Type 1 artifacts, as applied to a near infrared spectroscopic (NIRS) time series. The data exhibits artifacts due to eye blinks. Signals corresponding to $(\lambda_0^*, 0)$ and $(0, \lambda_1^*)$ are shown in Figs. 3(b, c). With (λ_0, λ_1) set using (5) with $\theta = 0.05$, we obtain an apparently accurate estimate of the transient artifacts (Fig. 3(d)). The corrected time series is obtained by subtracting the estimated artifact signal $\hat{\mathbf{x}}$ from the original data (Fig. 3(e)). The algorithm run time was about 80 milliseconds.

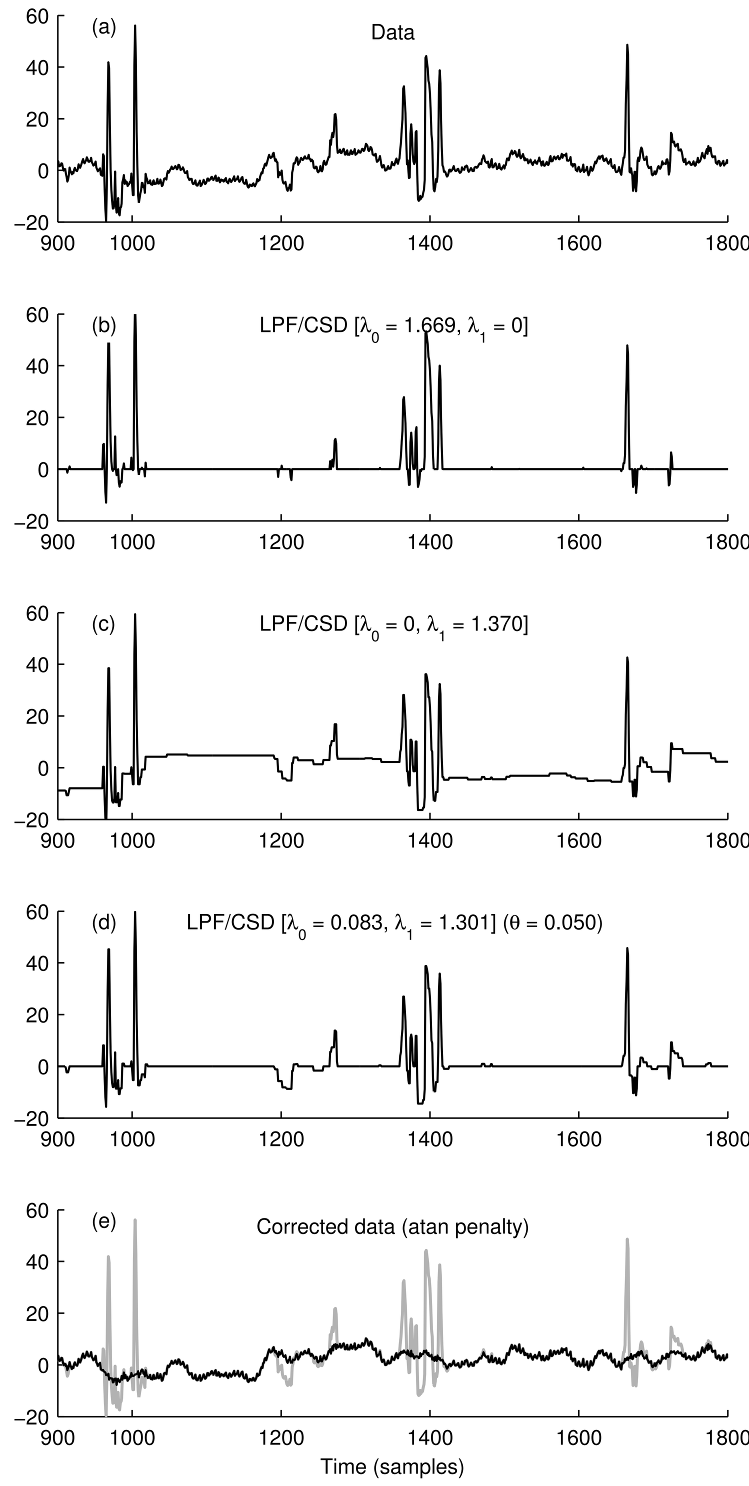

Figure 3: *Reduction of transient artifacts in NIRS time-series data. (a) Raw data. (b, c, d) Artifact estimation with $(\lambda_0^*, 0)$, $(0, \lambda_1^*)$, and (5). (e) Corrected data.*

5. Run times

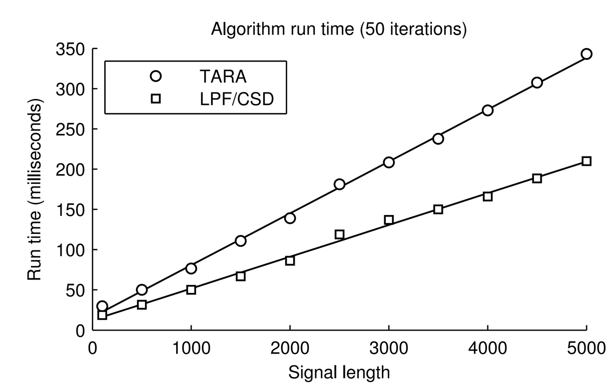

Run times measured using a 2013 MacBook Pro (2.5 GHz Intel Core i5) running Matlab R2011a.

6. Example 3

This example applies TARA to a simulated time series consisting of low-frequency sinusoids, additive rectangular pulses of short duration, several additive step discontinuities, and additive white Gaussian noise.

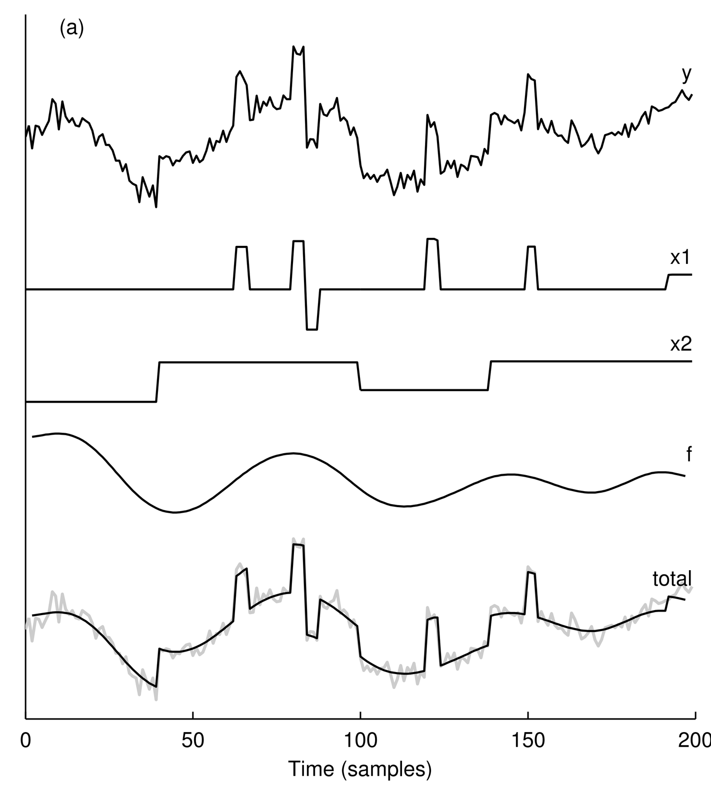

Figure 4: *Decomposition and filtering with TARA.*

7. Example 4

This example applies TARA to a NIRS time series acquired using a pair of optodes on the back of a subject's head. The data exhibits a motion-induced abrupt shift of the baseline, at time index 470. Other motion artifacts also are visible.

The Type 1 and Type 2 artifact signals as estimated by TARA, are sparse and approximately piecewise constant, as intended. The estimated total artifact signal appears to accurately model the artifacts present in the data. Note that the corrected time series has both low-frequency and high-frequency spectral content.

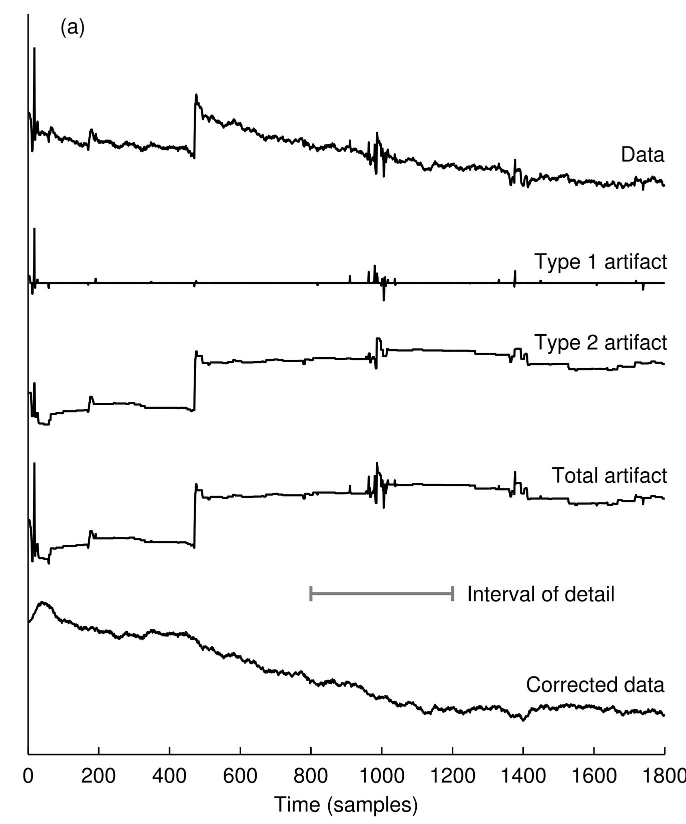

Figure 5: *Artifact reduction with TARA as applied to a NIRS time series.*

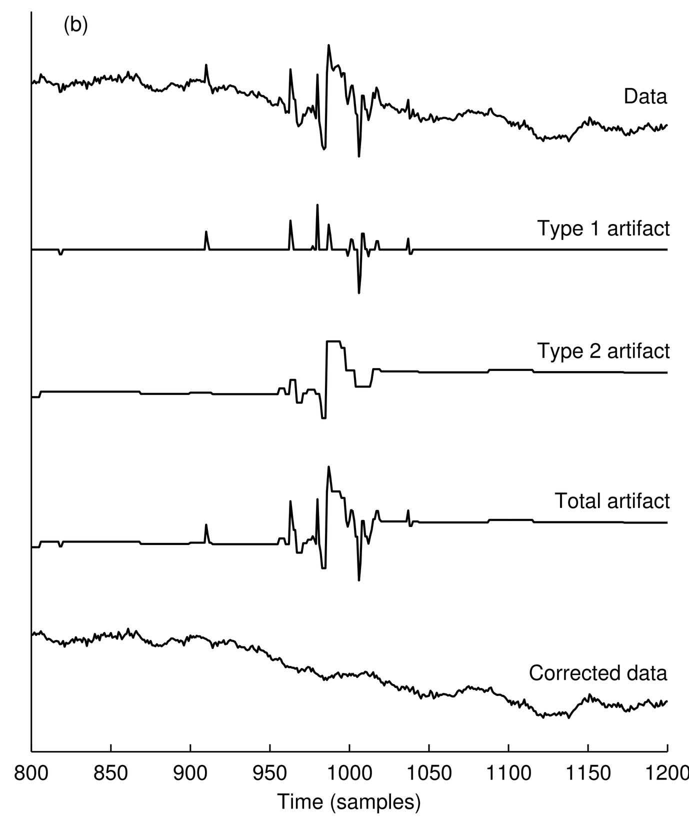

Figure 6: *Detail of Fig. 5*

Wavelet artifact estimation. Wavelet methods compare favorably to other methods for the correction of motion artifacts in single-channel NIRS time series [2, 4, 5]. In comparison with TARA, the wavelet method does not correct additive step discontinuities as well. The wavelet-estimated artifact signal smooths the additive step discontinuity.

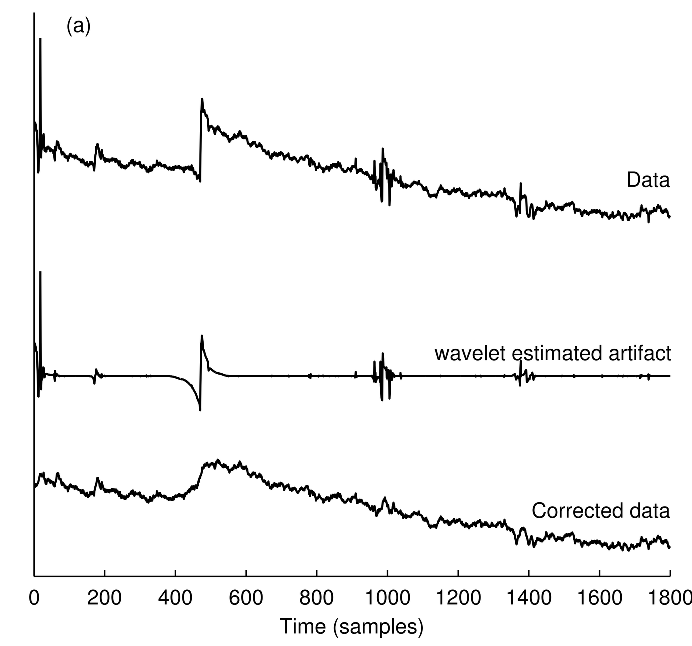

Figure 7: *Wavelet artifact estimation as applied to the NIRS time series shown in Fig. 5.*

References

[1] R. Al abdi, H. L. Graber, Y. Xu, and R. L. Barbour. Optomechanical imaging system for breast cancer detection. *J. Opt. Soc. Am. A*, 28(12):2473–2493, December 2011.

[2] S. Brigadoi et al. Motion artifacts in functional near-infrared spectroscopy: A comparison of motion correction techniques applied to real cognitive data. *NeuroImage*, 85:181–191, 2014.

[3] T. Fekete, D. Rubin, J. M. Carlson, and L. R. Mujica-Parodi. The NIRS analysis package: Noise reduction and statistical inference. *PLoS ONE*, 6(9):e24322, 2011.

[4] M. K. Islam, A. Rastegarnia, A. T. Nguyen, and Z. Yang. Artifact characterization and removal for *in vivo* neural recording. *J. Neuroscience Methods*, 226:110–123, 2014.

[5] B. Molavi and G. A. Dumont. Wavelet-based motion artifact removal for functional near-infrared spectroscopy. *Physio. Meas.*, 33(2):259, 2012.

This research was supported by the NSF under Grant No. CCF-1018020, the NIH under Grant Nos. R42NS050007, R44NS049734, and R21NS067278, and by DARPA project N66001-10-C-2008.